Proceedings of ASME Turbo Expo 2009: Power for Land, Sea and Air
GT2009
June 8-12, 2009, Orlando, Florida, USA

GT2009-59685

Global Turbulent Consumption Speeds ($S_{T,GC}$) Of H_2/CO Blends

Prabhakar Venkateswaran
School of Aerospace Engineering

Andrew D. Marshall
School of Mechanical Engineering

David R. Noble
School of Aerospace Engineering

Jose Antezana
School of Mechanical Engineering

Jerry M. Seitzman
School of Aerospace Engineering

Tim C. Lieuwen
School of Aerospace Engineering

Georgia Institute of Technology
Atlanta, GA 30332-0150

ABSTRACT

This paper describes measurements of the global turbulent consumption speed, $S_{T,GC}$, of atmospheric pressure H_2/CO flames at mean flow velocities and turbulence intensities up to U=50 m/s and u'/S_L =100, respectively. The particular emphasis of the paper is to characterize H_2/CO mixture properties upon turbulent flame speeds – a number of prior studies have noted that different fuels, with the same laminar flame speed and combusted in the same turbulent flow, can have widely different turbulent flame speeds. This effect is believed to be due to flame speed sensitivities to stretch and possibly thermo-diffusive instabilities. While this effect is widely known, little data are available for syngas blends.

Turbulent flame speeds were obtained with blends ranging from 30-90% H_2, with the mixture equivalence ratio, ϕ, adjusted at each fuel composition to have nominally the same laminar flame speed, S_L. In addition, equivalence ratio sweeps at constant H_2 level were also performed. The data clearly corroborate results from other studies that show significant sensitivity of $S_{T,GC}$ to fuel composition. In particular, at a fixed u' and S_L, values of $S_{T,GC}$ increase by almost a factor of 1.5 - 2 when H_2 levels are increased from 30% (at $\phi = 0.59$) to 90% (at $\phi = 0.46$). Moreover, $S_{T,GC}$ in the 90% H_2 case is 3 times larger than the $\phi = 0.9$ CH_4/air mixture with the same S_L value. An important conclusion from this work is that fuel effects on $S_{T,GC}$ highlighted above are not simply a low turbulence intensity phenomenon – they clearly persist over the entire range of turbulence intensities used in the measurements.

[*keywords:* syngas, hydrogen, turbulent flame speed, global consumption speed, Bunsen flames]

INTRODUCTION

There is significant interest in developing dry low NOx combustion technologies that can operate with synthetic gas (syngas) fuels derived from gasified coal or biomass [1]. Syngas fuels are typically composed primarily of H_2 and CO, and may also contain smaller amounts of CH_4, N_2, CO_2, H_2O, and other higher order hydrocarbons [2, 3]. However, the specific composition depends upon the fuel source and processing technique, leading to substantial variability in composition - one of the largest barriers towards their usage in lean, premixed combustion systems.

A variety of operability, emissions, and structural life issues must be addressed in evaluating the impact of fuel composition on a gas turbine combustor; e.g., NOx and CO emissions, liner and fuel nozzle thermal loading, blow-off and flashback limits, and combustion instabilities. The turbulent flame speed is an important parameter through which the fuel composition exerts influences on many of these issues, such as thermal loading, blow-off limits, flashback limits, and combustion instability [4]. For example, the turbulent flame speed has a direct impact on the flame length and its spatial distribution in the combustor. This, in turn, affects the thermal loading distribution on the combustor liners, fuel nozzles and other hardware. Furthermore, the flames proclivity to flashback is directly a function of how rapidly the flame propagates into the reactants, which is dependent on the turbulent flame speed. In addition, the turbulent flame speed has a leading order influence on combustion instability limits through its influence upon the flame shape and length [5]. For example, measurements from Santavicca [6] have clearly shown how

combustion instability boundaries are influenced by changes in flame location, due to changes in H_2 content of the fuel or mixture stoichiometry.

The laminar flame speed, S_L, is a thermo-physical property of a fuel-oxidizer mixture that describes the speed at which a laminar flame front propagates into a reactive mixture. For a given mixture, it is a function of pressure, temperature and flame stretch rate [7]. The turbulent flame speed, S_T, while having an analogous definition for the average propagation speed of a turbulent front, does not uniquely depend on the mixture's thermal and chemical properties. As with turbulence itself, S_T is a function of the flow within which the flame resides; i.e., it is a function of laminar flame speed, turbulence intensity, turbulence length scales, etc. Correlations of turbulent flame speed of the form $S_T = S_L \cdot f(u')$, where u' denotes the root mean square (RMS) turbulence fluctuation, have been obtained from numerous studies [8].

However, u' and S_L alone do not capture many important characteristics of S_T, a point that has been made repeatedly in the literature [8]. Fuel composition is also known to significantly influence the turbulent flame speed. For example, Kido *et al.* [9] obtained data for single-constituent fuels of H_2, CH_4, and C_3H_8. These fuel/air mixtures were diluted and operated at different stoichiometries in order to have the same laminar flame speeds. However, these fuels had substantially different turbulent flame speeds, with the high H_2 mixtures having an order of magnitude larger S_T value than the propane mixture. Thus, two different fuel mixtures having the same laminar flame speed, turbulence intensity and burner can have *appreciably* different turbulent flame speeds. Further compilations of data illustrating these effects can be found in the review of Lipatnikov and Chomiak [10].

These fuel effects are believed to be associated with flame instabilities and differential diffusion, leading to variations in the local consumption speed along the turbulent flame front. Differential diffusion occurs when there are differences in the relative rates of mass and/or thermal diffusion of the deficient species. Differential diffusion effects the local laminar flame speed and thermo-diffusive instability characteristics of the mixture [11]. This differential diffusion effect may be particularly important in the case of syngas fuels because of the large differences in diffusivity of the various fuel components (e.g., H_2 and CO, plus the diluents CO_2, N_2, and H_2O) with respect to each other and to air.

The measurements reported in this paper had two primary motivations. First, limited data are available for fuel mixtures, in particular, for mixtures of H_2 and CO. The variation of $S_{T,GC}$ with fuel composition for the physically interesting cases where the upstream turbulence intensity and flame temperature or flame speed are held constant, while relative fuel constituents are varied (H_2/CO ratio), is non-trivial and has not been previously measured. Second, much of the turbulent flame speed data have been obtained at relatively low turbulence intensities, u'/S_L values are often less than ten [12]. Measurements by Littlejohn and Cheng [13] at u'/S_L values up to 25 and Kido *et al.* [9] with u'/S_L values up to 25 suggest that these effects persist at higher turbulence intensities, but further data are needed to validate this point.

This paper reports measurements of global consumption speeds of H_2/CO mixtures. This paper's key contribution is obtaining data over a range of H_2/CO mixture compositions at turbulence intensities of up to u'/S_L =100. An important conclusion from this work is that fuel effects on $S_{T,GC}$ highlighted above are not simply a low turbulence intensity phenomenon – they clearly persist over the entire range of turbulence intensities used in the measurements.

EXPERIMENTAL APPROACH AND FACILITY

This section describes the approach and experimental facility used to quantify the turbulent flame speed. As noted above, $S_{T,GC}$ is a property of not only the fuel-air mixture, but also the flow. As such, well characterized, highly reproducible burners whose results can be compared to other workers and data are critical to these measurements [14].

We start with some discussion of the measurement approach. This is an important issue because of the definition dependence of S_T. Extensive discussion of the merits and drawbacks of various approaches are contained in the literature. Some resolution has been achieved in two recent reviews [12, 15] and through the International Workshop on Premixed Flames [16], where it is noted that there are actually multiple useful definitions for S_T that are relevant for different combustion issues (e.g., flashback versus heat release per volume). Four definitions of S_T have been proposed: local displacement speed, $S_{T,LD}$, global displacement speed, $S_{T,GD}$, local consumption speed, $S_{T,LC}$, and global consumption speed, $S_{T,GC}$ [12, 15, 16]

The local consumption and displacement speeds attempt to quantify the local propagation rate and mass burning rate of the turbulent front, respectively. There are various problems associated with defining these quantities locally, however. For example, the definition of $S_{T,LC}$ is:

$$S_{T,LC} = S_{L0} I_0 \int_{-\infty}^{\infty} \Sigma d\eta \qquad (1)$$

where S_{L0}, I_0 and Σ are the unstrained laminar flame speed, stretch factor and the flamelet surface area per unit volume respectively. Clearly, this integral is a function of the integration path, η, through the turbulent flame brush. Several authors suggest that it be performed in a direction normal to the flame brush [12], which is itself usually a function of reaction progress variable.

Difficulties associated with defining a local value of S_T can be circumvented to some extent by defining global burning rates (assuming, of course, that all the reactant mass flow pass

through the flame brush [12]), at the cost of averaging over potentially substantial variations in local burning rates for cases where the flame brush is spatially evolving. However, global turbulent flame speeds are also definition dependent. For example, $S_{T,GC}$ is defined as:

$$S_{T,GC} = \frac{\dot{m}_R}{\rho_R \bar{A}_{<c>}} \tag{2}$$

where $\dot{m}_R$, ρ_R and $\bar{A}_{<c>}$ denote reactant mass flow rate, reactant density and mean flame area corresponding to some prescribed $<c>$ contour. Thus, the value of $S_{T,GC}$ is itself a function of which progress variable surface is used to define the mean flame front area.

This study focuses upon measurements of $S_{T,GC}$ using a turbulent Bunsen flame, an $S_{T,GC}$ measurement approach recommended by Gouldin and Cheng [16]. This configuration was used because of the wide variety of available data in similar geometries for benchmarking and comparisons.

A schematic of the system is shown in Figure 1. The burner is a smoothly contoured nozzle with high contraction ratio and a 20 mm exit diameter. The contoured nozzle inhibits boundary layer growth in order to have a top hat exit velocity profile. An annular sintered plate is placed around the burner outlet to hold a premixed, methane-air pilot flame, to stabilize the main flame. The total mass flow rate of the pilot does not exceed 5% of the main flow rate to ensure minimal impact of the pilot on the main flame.

Mass flow rates of the fuel and air for both the main and pilot flames are metered using mass flow controllers that have accuracies of ±1.5% of the full scale. As a result, equivalence ratios quoted here have uncertainties ranging from 3% to 5%, depending on the full-range scale of the mass flow controllers used.

The fuel/air mixture is premixed 2 m ahead of the burner. Upon entering the main burner assembly, the flow passes through a layer of ball bearings to minimize "jetting" effects from the smaller diameter reactant feed lines.

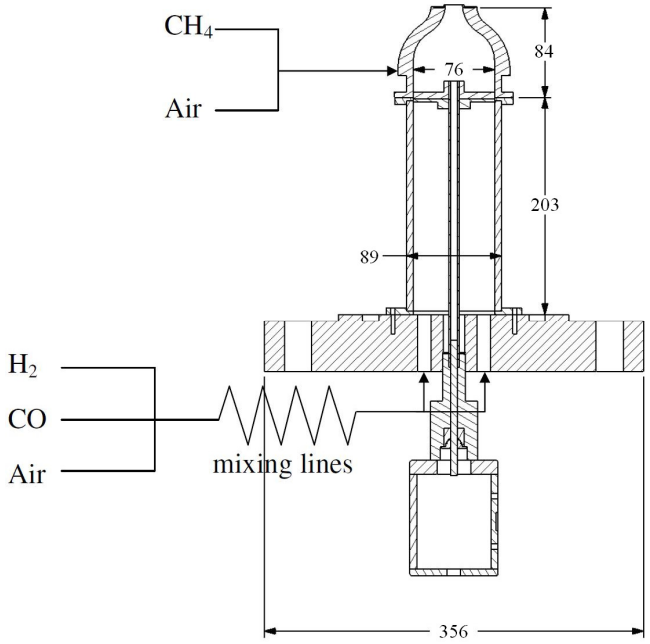

Figure 1: Schematic of the experimental facility. Dimensions in mm.

The turbulence intensity is varied independently of the mean flow velocity using a remotely controlled turbulence generator. This turbulence generator assembly consists of milled slots in a thin plate that cause flow separation and vorticity generation as the flow passes through them, as described by Videto and Santavicca [17], Cheng and co-workers [18], and Kortschik and Plessing [19]. These vortical structures impinge on the inclined wall of the converging section of the nozzle, breaking them down into finer turbulent eddies.

As shown in Figure 1, the turbulence generating plates are secured 84 mm upstream of the burner exit. Prior implementations of these turbulence generators use fixed plates – different blockage ratio plates were manufactured to vary turbulence intensity. In this study, substantial effort was devoted to developing a system that is continuously variable. This capability is needed to facilitate the high pressure measurements which are planned for the next phase of experiments. This system consists of a 3 mm thick bottom plate that is secured to the plenum and a 6 mm thick top plate attached to a central shaft that is connected to a stepper motor. This configuration allows for variable degrees of blockage as shown in Figure 2.

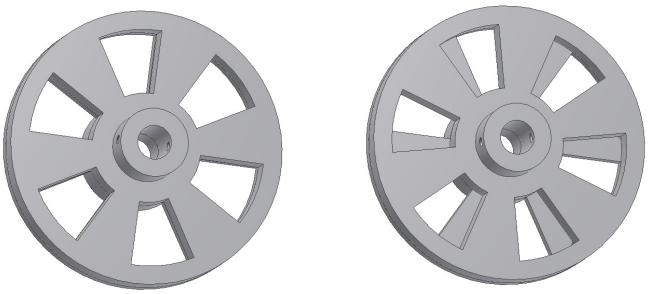

(a) (b)

Figure 2: Schematic of the turbulence generating plates: a) fully open and b) partially closed.

The plate's angular position is measured with an optical encoder to an accuracy of ±0.1°. The stepper motor is connected to the central shaft via a worm gear, minimizing backlash. Maximum and minimum blockage possible with this setup is 97% and 69%, corresponding to an angular opening of 1.5 degrees and 30 degrees, respectively. Turbulence intensity increases monotonically with increasing blockage ratio.

At very high blockage ratios, the mixture passes through the slots at an angle, leading to substantial swirl in the flow. This effect was reduced somewhat by the addition of straighteners, see Figure 3, but it still imposes a maximum blockage ratio over which data are obtained. We utilized the criterion that the maximum blockage ratio remain less than 93% for all flame speed data presented in this paper.

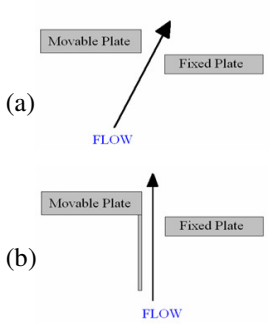

Figure 3: Flow characteristics (a) without and (b) with flow straighteners.

Flow Field Characterization

The flow field was characterized using a TSI 3-component Laser Doppler Velocimetry (LDV) system. The flow was seeded using 5 µm alumina (Al_2O_3) particles. Data were obtained at mean flow velocities from U = 4 – 50m/s, which correspond to $Re_D = \frac{UD}{\upsilon} = 5100 - 64{,}000$.

Figure 4 through Figure 6 plot representative profiles of the mean and fluctuating axial, radial and azimuthal velocities as a function of the radial distance from the center of the 20mm diameter burner at 50m/s at three different blockage ratios.

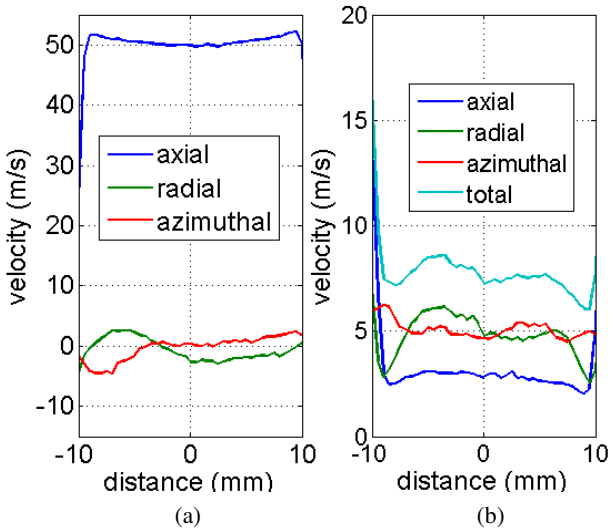

(a) (b)

Figure 4: Plots of a) mean axial, radial and azimuthal velocities and b) fluctuating axial, radial, and azimuthal and total fluctuating velocities as a function of radial distance from center of the burner for U = 50m/s at a blockage ratio of 69%.

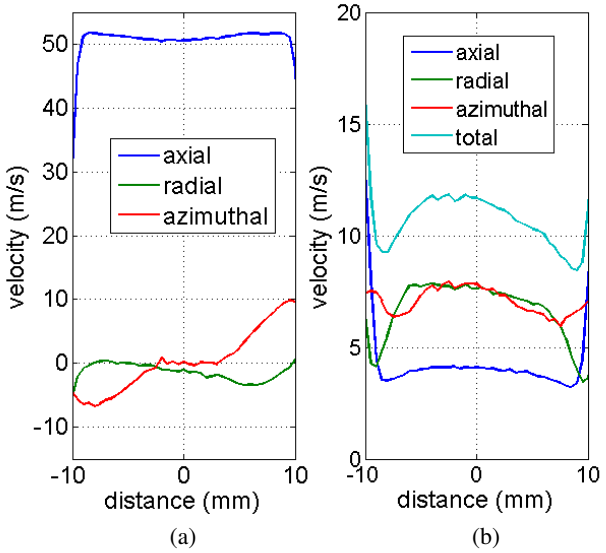

(a) (b)

Figure 5: Plots of a) mean axial, radial and azimuthal velocities and b) fluctuating axial, radial, and azimuthal and total fluctuating velocities as a function of radial distance from center of the burner for U = 50m/s at a blockage ratio of 81%.

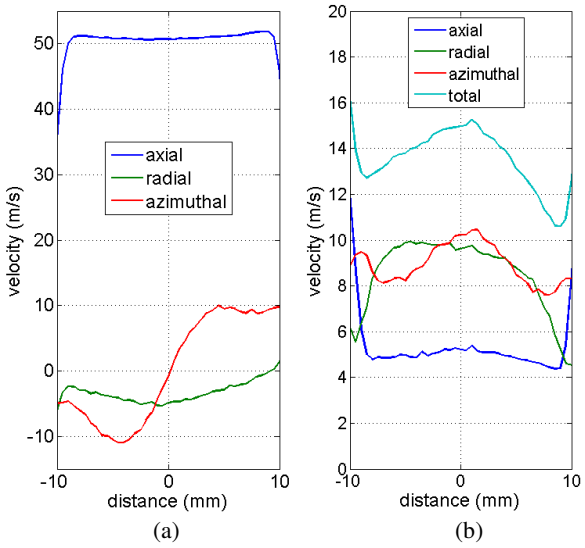

Figure 6: Plots of a) mean axial, radial and azimuthal velocities and b) fluctuating axial, radial, and azimuthal and total fluctuating velocities as a function of radial distance from center of the burner for U = 50m/s at a blockage ratio of 93%.

The data show a well-defined top-hat mean axial velocity, along with low radial velocity. The azimuthal velocity increases with increasing blockage ratio, as discussed earlier. It should be noted that the time averaged mean and fluctuating velocities are flat, except in the boundary layer, and that as the blockage ratio is increased from 69% in Figure 4 to 93% in Figure 6, the turbulence intensity increases.

Figure 7 summarizes the performance of the turbulence generator, by plotting the turbulence intensity, u'/U as a function of the blockage ratio.

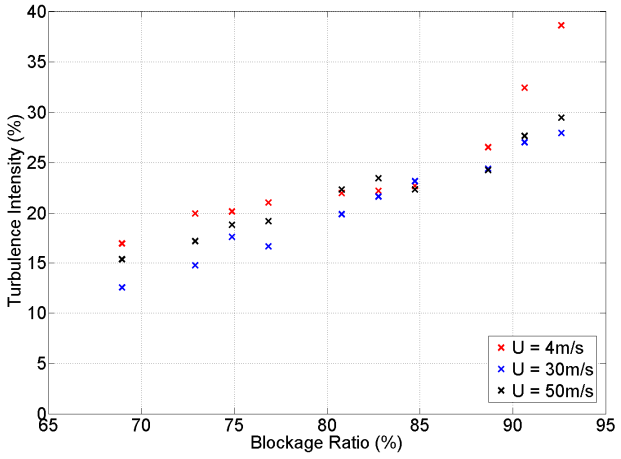

Figure 7: Dependence of burner centerline total turbulence intensity (i.e. summed over all 3 fluctuating velocity components) upon blockage ratio.

Limited particle image velocimetry (PIV) studies of the cold-flow velocity field were also conducted. Figure 8 shows the mean and RMS velocity fields normalized by the mean centerline velocity at the burner exit. Note that the centerline turbulence intensity remains relatively constant, and actually grows slightly, for at least the first 50 mm downstream.

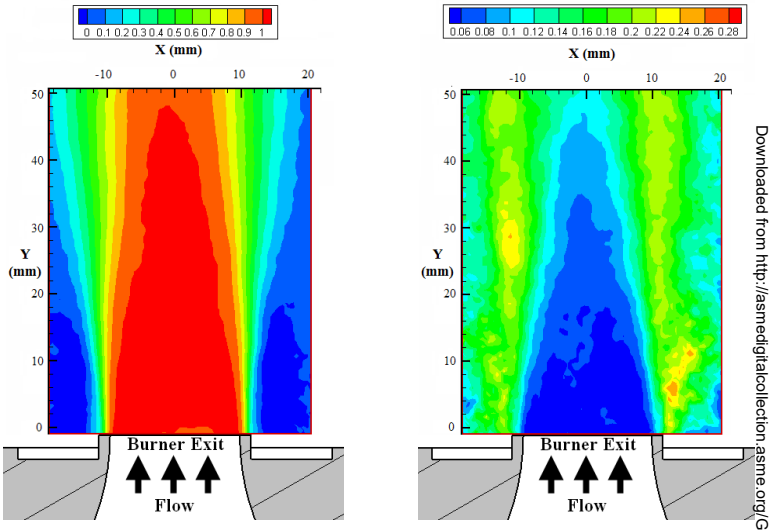

Figure 8: PIV velocity data for the 20mm burner at a blockage ratio of 80% for U = 4m/s a) mean velocity normalized by the centerline mean velocity at the burner exit b) RMS velocity normalized by the centerline mean velocity at the burner exit.

Figure 9 presents typical 1-D turbulent power spectra at the burner centerline for several blockage ratios at U = 4 m/s. The data were obtained from autocorrelations of the LDV time series, described later. The spectra show a smooth roll-off with increasing frequency, and that there are no discrete peaks, as desired. The graph shows that the power spectrum values increases with blockage ratio.

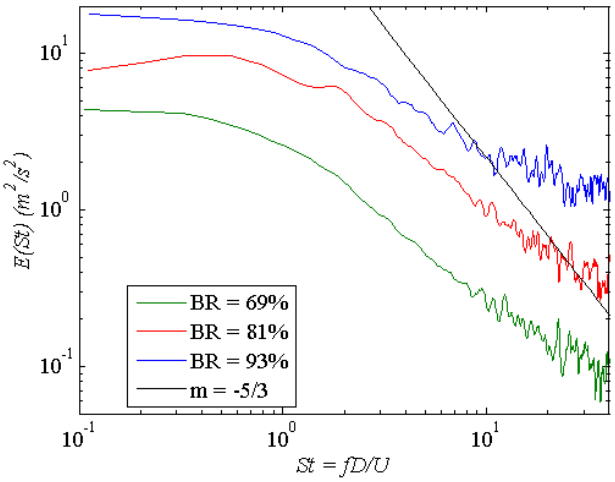

Figure 9: 1-D turbulent power spectra as a function of Strouhal number St for U = 4m/s at 3 different blockage ratios.

Integral time scales, t_{int}, were determined from autocorrelations of the centerline velocity data. The

autocorrelation function was determined from Equation (3) using the slotting technique of Mayo [20] with the local normalization improvement described by Tummers [21]:

$$\rho(k\Delta\tau) = \frac{\sum_{i=1}^{N-1}\sum_{j=i+1}^{N} u_i u_j (k\Delta\tau)}{\sqrt{\sum_{i=1}^{N-1} u_i^2 (k\Delta\tau) \sum_{j=i+1}^{N} u_j^2 (k\Delta\tau)}} \quad (3)$$

for: $k = 0,1,...,M-1$

where $\left(k-\frac{1}{2}\right)\Delta\tau < t_i - t_j < \left(k+\frac{1}{2}\right)\Delta\tau$, $M-1 = \frac{\tau_{\max}}{\Delta\tau}$, $\tau_{\max}$ is the maximum lag time, and $\Delta\tau$ is the slot width. The integral time scale was defined using the relationship:

$$t_{\text{int}} = \int_0^{\infty} \rho(\tau) d\tau \quad (4)$$

Because of the high uncertainties associated with the autocorrelation at large time lags (because of its low value), an exponential expression of the form $\rho(\tau) = ae^{-b\tau} + (1-a)e^{-c\tau}$ was fit to the autocorrelation function and used to evaluate this integral, so that t_{int} is given by Equation (5). A typical result is shown in Figure 10.

$$t_{\text{int}} = \frac{a}{b} + \frac{1-a}{c} \quad (5)$$

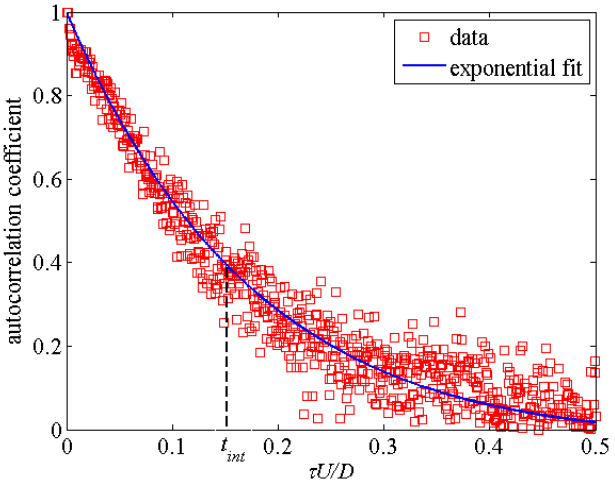

Figure 10: Autocorrelation coefficient plotted against normalized lag time for U = 4m/s, blockage ratio = 93%.

These integral time scales were converted to integral length scales, l_{int}, using the relation $l_{int} = t_{int}U$, as per Taylors' hypothesis. Figure 11 summarizes the calculated l_{int}/D values at mean flow velocities of 4, 30, and 50 m/s at various blockage ratios. The data indicate that l_{int}/D is nearly constant at 30 and 50 m/s, and changes slightly with blockage ratio. The data show that turbulence length scales are not varying with blockage gap width and therefore, that the associated variations in turbulence intensity are at essentially constant integral length scale. The t_{int} values in the 4 m/s case are substantially higher in value and do indicate a larger sensitivity to blockage ratio. It is assumed that this reflects a different characteristic of the turbulence generator system at the much lower Reynolds numbers these data were obtained. This result will be studied further in future studies of velocity characteristics at other flow conditions.

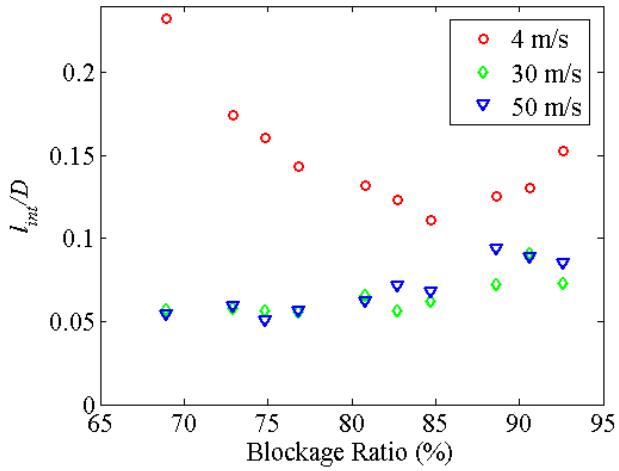

Figure 11: Comparison of integral length scale (normalized by burner diameter) vs. blockage ratio at 4, 30, and 50m/s.

Image Analysis

Global consumption speeds were calculated using Equation (2), whose key measurement input is progress variable surface area, $\overline{A}_{<c>}$. This section describes the approach used to determine this surface area.

Digital images of the flame emission are captured with a 16-bit intensified charge-coupled device (ICCD) camera with a resolution of 512 x 512 pixels and a 105mm, f/4.5, UV camera lens. The camera system is sensitive in the visible and ultraviolet regions (~220 – 650nm) and, hence, is capable of capturing both OH* and CO_2* chemiluminescence. This is important for high hydrogen content fuels since the OH* chemiluminescence associated with hydrogen flames emits in the UV range.

Line of sight images of the flame were obtained over 5 seconds and time averaged, see Figure 12(a). These averaged images are nearly symmetric about the centerline. The left and right halves were then averaged, see Figure 12(b), and filtered with a 2-D median filter with a kernel size that is less than 2% of the burner diameter. To estimate the time averaged, two-dimensional flame brush location from the line-of-sight images, a three-point Abel deconvolution scheme [22] was used, see Figure 12(c). The axial distribution of the centerline intensity is then fit to a Gaussian curve, from which the location of the maximum intensity is identified. This point is associated with the most probable location of the flame, and defined as the <c> = 0.5 progress variable contour. The estimated uncertainty in

identifying this point is 1-2%. The other progress variables were then defined by the relation:

$$< c >= \begin{cases} \dfrac{I}{I_{\max}} & < c > \ \le \ 0.5 \\ 1 - \dfrac{I}{I_{\max}} & < c > \ > \ 0.5 \end{cases} \qquad (6)$$

Straight lines are then drawn from this point to the two flame anchoring points and rotated about the line of symmetry to generate a cone. The <c> = 0.5 surface is drawn in Figure 12(c).

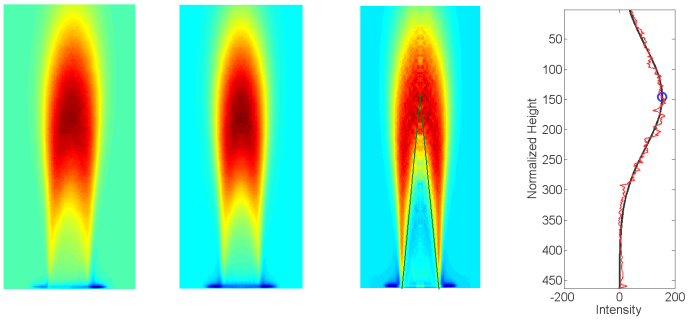

(a) (b) (c) (d)

Figure 12: Time averaged, line of sight flame images showing (a) background subtracted image, (b) axisymmetric image and (c) Abel inverted image with <c> = 0.5 contour shown (d) plot of intensity as a function of image height used to determine contours. The red and black lines represent the raw data and fitted data respectively.

From Figure 12 it is clear that the surface used to determine $\overline{A}$ does not coincide with the actual flame <c>=0.5 surface except at the centerline. However, this method was used to aid in comparing the results of this study with other data in the literature where a similar method was used to determine the flame area (e.g., the "angle method") [14, 23] . In future publications we will report the sensitivity of the results to this surface location; however, we believe that all trends observed will remain unaltered.

As noted earlier, $S_{T,GC}$ is a function of the progress variable, <c>, used to define $\overline{A}$. Figure 13 plots the dependence of $S_{T,GC}$ upon the progress variable contour, <c>, at several H_2/CO ratios. As expected, $S_{T,GC}$ decreases with increasing <c> value. This graph also shows that the different H_2/CO ratio flames have similar dependence upon <c> contour. It also shows, however, that the highest H_2 mixture (90/10 mixture), does have the least sensitivity to <c>, illustrating that the flame brush thickness is decreasing with increased H_2 content.

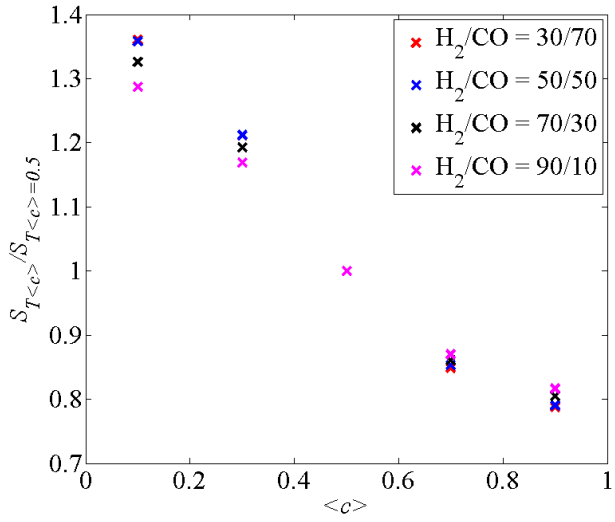

Figure 13: Dependence of $S_{T,GC}$ value upon using different progress variable normalized by $S_{T,GC<c>=0.5}$ as a function of the progress variable for different H_2/CO ratios at 50m/s and u'/S_L = 22.5, and S_L = 0.34m/s.

The overall uncertainty in the estimated $S_{T,GC}$ (as defined in this paper) value is then estimated to be 3%.

RESULTS AND DISCUSSION

Two basic sets of tests were performed. First, measurements of $S_{T,GC}$ were obtained as a function of u'/S_L at mean flow velocities of 4, 10, 30, and 50m/s and H_2/CO ratios ranging from 30/70-90/10. The quoted turbulence intensity is equal to the total (i.e., all three velocity components included) value at the burner centerline at the exit. These H_2/CO sweeps were performed at nominally constant laminar flame speed, S_L = 34cm/s, by adjusting mixture stoichiometry at each H_2/CO ratio. These S_L estimates were determined using CHEMKIN software with the Davis H_2/CO mechanism [24]. In addition, a CH_4/air data set was also obtained at ϕ = 0.9 for comparison at the same S_L. A uniform symbol type and color scheme was used for these tests, as summarized in Table 1.

The second set of tests was performed by sweeping equivalence ratio at constant H_2/CO ratio values of 30/70 and 60/40. The parameter ranges explored in this study are summarized in Table 2 below.

Table 1: Legend used for constant S_L H_2/CO sweeps data.

H_2 (%) \ Velocity (m/s)	4	10	30	50
30	◇	□	○	×
50	◇	□	○	×
70	◇	□	○	×
90	◇	□	○	×
CH_4	◇	□	○	

Table 2: Investigated parameter space.

	Constant S_L				ϕ Sweep					CH_4
U (m/s)	4, 10, 30, 50									4, 10, 30
H_2 (%)	30	50	70	90	30		60			0
ϕ	0.59	0.53	0.50	0.46	0.7	0.8	0.4	0.6	0.8	0.9
S_L (m/s)	0.34				0.48	0.59	0.15	0.51	0.90	0.34

H_2/CO Sweeps at Constant S_L

This section presents data at various H_2/CO ratios at nominally constant S_L. This data set is summarized in Figure 14 and Figure 15, which plot $S_{T,GC}/S_L$ for H_2/CO mixtures of 30/70, 50/50, 70/30, and 90/10 and mean flow velocities of 4, 10, 30, and 50 m/s. These two graphs plot the same data on a linear (Figure 14) and log (Figure 15) scale. For a given fuel composition, $S_{T,GC}$ increases monotonically with turbulence intensity. Moreover, some dependence of $S_{T,GC}$ on mean flow velocity is also observed, but this is not large. The main observation from this data is the monotonically increasing value of $S_{T,GC}$ with H_2 levels. Moreover, the data indicate that these fuel effects persist even at very high turbulence intensities.

Also included on these graphs are several measured or predicted S_T correlations. Some caution should be exercised in comparing these with the data, because of the definition dependence of S_T noted earlier. Bradley's equation [25] is given by:

$$\frac{S_T}{S_L} = 1.52\frac{u'}{S_L} \tag{7}$$

This is a theoretical result derived from considerations of the fractal characteristics of high intensity turbulent flames. It was derived using theoretically and experimentally obtained values for the fractal dimension and turbulent dissipation coefficients. As a result, the analysis appears to lend itself to a local definition of turbulent flame speed such as $S_{T,LC}$ or $S_{T,LD}$. A similar expression, derived from a different theoretical approach, was proposed by Anand and Pope [26], with a constant of 1.5.

Schelkin's expression [27] is given by:

$$\frac{S_T}{S_L} = \left[1+\left(2\frac{u'}{S_L}\right)^2\right]^{0.5} \tag{8}$$

This is also a theoretical result that most closely corresponds to $S_{T,LC}$ or $S_{T,LD}$ using Damkohler's approach to wrinkled flames where the turbulent structures are much larger than the laminar flame thickness [25].

Yakhot [28] also developed the following theoretical expression, valid again for high turbulence intensity flames using renormalization approaches. Again, this expression most closely corresponds to $S_{T,LC}$ or $S_{T,LD.}$

$$\frac{S_T}{S_L} = \exp\left[\left(\frac{S_T}{S_L}\right)^2 \Big/ \left(\frac{u'}{S_L}\right)^2\right] \tag{9}$$

Kobayashi et al. [29] developed a correlation from experimental data for CH_4/air and C_2H_4/air turbulent Bunsen flames that included pressure effects.

$$\frac{S_T}{S_L} = 2.9\left[\left(\frac{P}{P_0}\right)\left(\frac{u'}{S_L}\right)\right]^{0.38} \tag{10}$$

This value of S_T was based upon the $<c>$ = 0.5 contour. Figure 14 and Figure 15 show that the correlation over-predicts $S_{T,GC}$ for our CH_4/air data, but generally follows the observed trend. One possibility for this is that the u' quoted by Kobayashi *et al.* [14] is only the axial RMS, while u' used in the current study is the total RMS which includes axial as well as radial and azimuthal components. Under the assumption that the u' quoted by Kobayashi only included axial RMS fluctuations and assuming they had isotropic turbulence, the correlation was adjusted to include all three components of the RMS fluctuations. This new curve fit is labeled "Kobayashi (isotropic)" in Figure 14. In order to examine this effect further, the relationship between our axial RMS and total RMS was found to be $u'_{axial} = u'/3$. This relationship was then used to again adjust the u' values reported by Kobayashi to be comparable to those used in the current study. This curve is labeled "Kobayashi (adjusted)". As shown in Figure 14, both of the adjusted correlations under-predict the values found, however, the original correlation of Kobayashi and the one adjusted for isotropic turbulence bracket the CH_4 values obtained in this experiment.

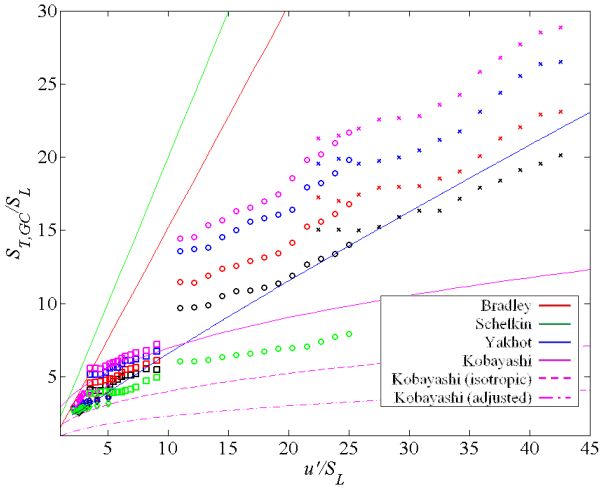

Figure 14: Variations of turbulent flame speed, S_T, with turbulence intensity, u', normalized by S_L at various mean flow velocities and H_2/CO ratios (linear plot).

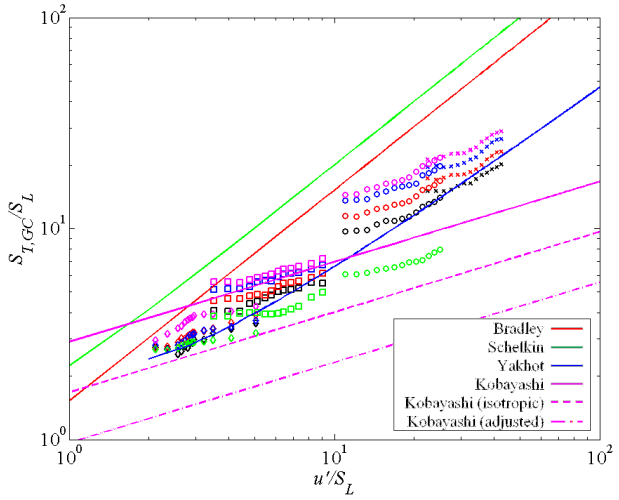

Figure 15: Variations of turbulent flame speed, $S_{T,GC}$, with turbulence intensity, u', normalized by S_L at various mean flow velocities and H_2/CO ratios (log-log plot).

The effects of H_2 level upon $S_{T,GC}/S_L$ at a fixed turbulence intensity is plotted in Figure 16. This graph shows an essentially linear dependence of $S_{T,GC}/S_L$ upon H_2 levels in the fuel over the investigated range. The point at 0% H_2 corresponds to the CH_4 flame. Note that the difference in flame speeds between low and high H_2 flames for the H_2/CO blends and the CH_4/air and H_2/CO/air flames is significant, being as large as two and three, respectively.

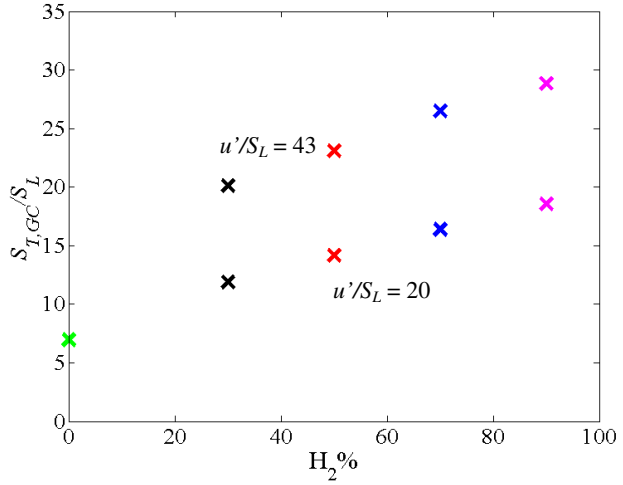

Figure 16: S_T/S_L variation with H_2 content for u'/S_L = 20 and 43 at S_L = 0.34m/s.

Equivalence Ratio Sweeps

In order to determine the effect of equivalence ratio on a specific fuel blend, H_2 content was fixed (30 and 60%) for three equivalence ratios. The symbols used for Figure 17 through Figure 20 are presented in Table 3. Figure 17 and Figure 18 show the results for a 60% H_2 mixture at ϕ = 0.4, 0.6, 0.8 for mean flow velocities of 4, 10, 30, and 50 m/s. Note that S_L is not held nominally constant for these data, as it was in the prior section.

Table 3: Legend for constant H_2 content equivalence ratio sweeps data

H_2	ϕ	Velocity (m/s) 4	10	30	50
30%	0.59	◇	□	○	×
	0.7	◇	□	○	×
	0.8	◇	□	○	×
60%	0.4	◇	□	○	×
	0.6	◇	□	○	×
	0.8	◇	□	○	×

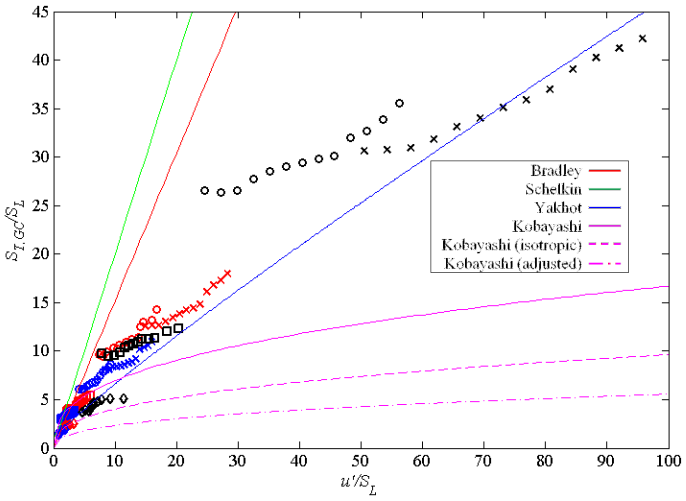

Figure 17: Variations of turbulent flame speed, $S_{T,GC}$, with turbulence intensity, u', normalized by S_L at various mean flow velocities and equivalence ratios at a fixed H_2 content of 60% (linear plot).

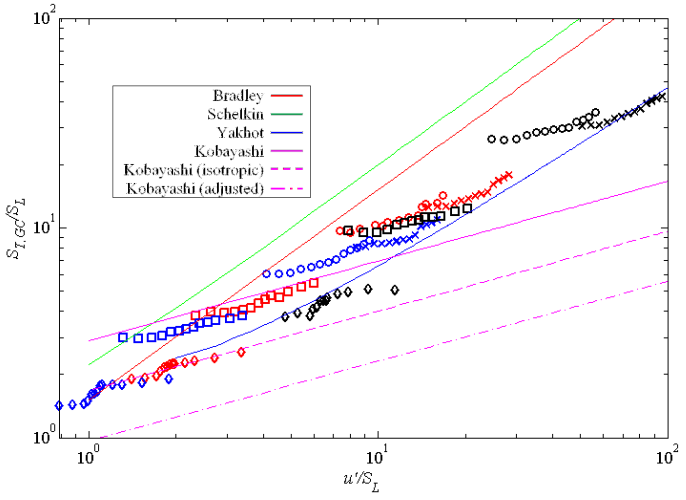

Figure 18: Variations of turbulent flame speed, $S_{T,GC}$, with turbulence intensity, u', normalized by S_L for various mean flow velocities and equivalence ratios at a fixed H_2 content of 60% (log-log plot).

As in Figure 14 and Figure 15, the S_T correlations discussed above have also been plotted. From Figure 18, which is the log-log version of Figure 17, it is seen that the data generally fall within the band formed by the correlations given

by Equation (7) and Equation (9). Furthermore, the slope of the data seems to agree quite well with Kobayashi's correlation, given by Equation (10), particularly at the low to intermediate u'/S_L ranges.

Figure 19 shows the results for a 30% H_2 mixture at ϕ = 0.59, 0.7, 0.8 for mean flow velocities of 4, 10, 30, and 50 m/s.

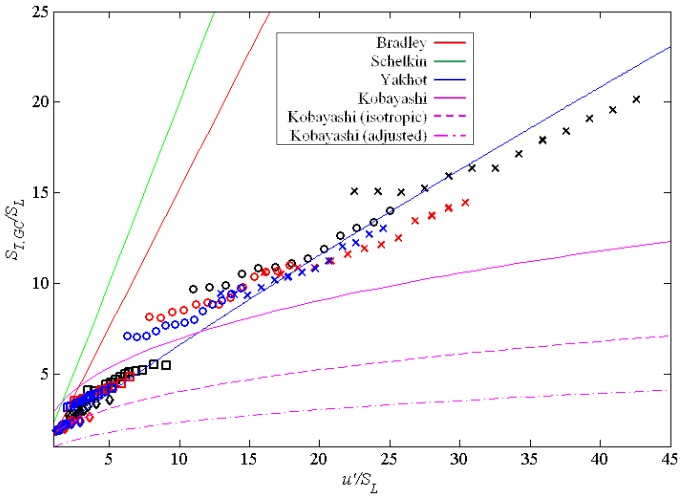

Figure 19: Variations of turbulent flame speed, $S_{T,GC}$, with turbulence intensity, u', normalized by S_L at various mean flow velocities and equivalence ratios at a fixed H_2 content of 30% (linear plot).

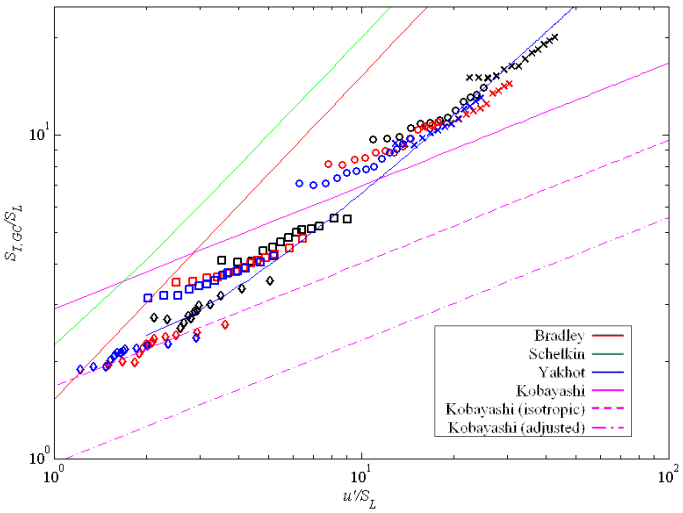

Figure 20: Variations of turbulent flame speed, $S_{T,GC}$, with turbulence intensity, u', normalized by S_L at various mean flow velocities and equivalence ratios at a fixed H_2 content of 30% (log-log plot).

Again from Figure 20, it can be seen the data generally fall within the band created by the stretch-free correlations. Furthermore, since the u'/S_L range investigated with the 30/70 H_2/CO mixture is smaller, it is easier to see that the correlation given by Equation (9) is a close match.

CONCLUDING REMARKS

These data clearly corroborate results from other studies that show significant sensitivity of $S_{T,GC}$ to fuel composition. For example, $S_{T,GC}$ in the 90% H_2 case is 3 times larger than the ϕ=0.9 CH_4/air mixture with the same S_L value. An important conclusion from this work is that fuel effects on S_T highlighted above are not simply a low turbulence intensity phenomenon – they clearly persist over the entire range of turbulence intensities used in the measurements.

Work is ongoing in two primary directions. First, we are obtaining similar data with another burner diameter (D=12 mm) to assess length scale effects. In addition, we are planning measurements with reactant preheat and at higher pressures. Second we are quantifying the evolution of the turbulent flame brush thickness. Finally, we are working toward physics based correlations of these data, utilizing the differential diffusion correlation approach from Kido *et al.*[30, 31].

NOMENCLATURE

$\overline{A}_{<c>}$	Mean flame area associated with given <c> contour
<c>	Progress variable contour
D	Burner diameter
I	Intensity
I_0	Stretch factor
I_{max}	Maximum intensity
P	Pressure
P_0	Standard pressure
Re_D	Reynolds number
S_L	Laminar flame speed
S_{L0}	Unstrained laminar flame speed
S_T	Turbulent flame speed
$S_{T,GC}$	Global turbulent consumption speed
$S_{T,GD}$	Global turbulent displacement speed
$S_{T,LC}$	Local turbulent consumption speed
$S_{T,LD}$	Local turbulent displacement speed
U	Mean flow velocity (derived from volume flow rate)
l_{int}	Integral length scale
$\dot{m}_R$	Reactant mass flow rate
t_{int}	Integral time scale
u'	Root mean square turbulence fluctuations
u'_{axial}	Axial root mean square turbulence fluctuations
$\rho(k\Delta\tau)$	Autocorrelation function
ρ_R	Reactant density
Σ	Flamelet surface area per unit volume

τ_{max}	Maximum lag time
$\Delta\tau$	Slot width
ϕ	Equivalence ratio

ACKNOWLEDGEMENTS

This research was partially supported by University Turbine Systems Research program, Mark Freeman, contract monitor, under contract DE-FC21-92MC29061. It was also supported by Siemens Energy through a sub-contract with DOE prime contract DE-FC26-05NT42644, Dr. Scott Martin contract monitor.

The authors gratefully acknowledge Mr. Juan Camilo Pedroza and Mr. Milad Navaei for their assistance in assembling the experimental facility and data collection.

REFERENCES

1. Lieuwen, T., Yang, V., *Syngas Combustion*. 2009: CRC Press.
2. Klimstra, J., *Interchangeability of Gaseous Fuels ? The Importance of the Wobbe-Index.* SAE transactions, 1986. **95**(6): p. 962-972.
3. Moliere, M., *Benefiting From the Wide Fuel Capability of Gas Turbines: A Review of Application Opportunities.* ASME Paper# GT-2002-30017, 2002.
4. Lieuwen, T., McDonell, V., Petersen, E., Santavicca, D., *Fuel Flexibility Influences on Premixed Combustor Blowout, Flashback, Autoignition, and Stability.* Journal of Engineering for Gas Turbines and Power, 2008. **130**: p. 011506.
5. Lieuwen, T.C., Yang, V., *Combustion Instabilities in Gas Turbine Engines (Operational Experience, Fundamental Mechanisms and Modeling).* Progress in Astronautics and Aeronautics, 2005.
6. Figura, L., Lee, J.G., Quay, B.D., Santavicca, D. , *The Effects of Fuel Composition on Flame Structure and Combustion Dynamics in a Lean Premixed Combustor*, in *ASME Paper # GT2007-27298*. 2007.
7. Vagelopoulos, C.M., Egolfopoulos, F. N., *Laminar Flame Speeds and Extinction Strain Rates of Mixtures of Carbon Monoxide with Hydrogen, Methane, and Air.* Symposium (International) on Combustion, 1994. **25**(1): p. 1317-1323.
8. Lipatnikov, A.N., Chomiak, J., *Turbulent Flame Speed and Thickness: Phenomenology, Evaluation, and Application in Multi-Dimensional Simulations.* Progress in Energy and Combustion Science, 2002. **28**(1): p. 1-74.
9. Kido, H., Nakahara, M., Nakashima, K., Hashimoto, J., *Influence of Local Flame Displacement Velocity on Turbulent Burning Velocity.* Proceedings of the Combustion Institute, 2002. **29**(2): p. 1855-1861.
10. Lipatnikov, A.N. and J. Chomiak, *Molecular Transport Effects on Turbulent Flame Propagation and Structure.* Progress in Energy and Combustion Science, 2005. **31**(1): p. 1-73.
11. Law, C.K., Jomaas, G., Bechtold, J. K., *Cellular Instabilities of Expanding Hydrogen/Propane Spherical Flames at Elevated Pressures: Theory and Experiment.* Proceedings of the Combustion Institute, 2005. **30**(1): p. 159-167.
12. Driscoll, J.F., *Turbulent Premixed Combustion: Flamelet Structure and its Effect on Turbulent Burning Velocities.* Progress in Energy and Combustion Science, 2008. **34**(1): p. 91-134.
13. Littlejohn, D., Cheng, R. K., *Fuel Effects on a Low-Swirl Injector for Lean Premixed Gas Turbines.* Proceedings of the Combustion Institute, 2007. **31**(2): p. 3155-3162.
14. Kobayashi, H., Tamura, T., Maruta, K., Niioka, T., Williams, F. A. *Burning Velocity of Turbulent Premixed Flames in a High-Pressure Environment*. 1996: Combustion Institute.
15. Cheng, R., K., *Turbulent Combustion Properties of Premixed Syngases*, in *Syngas Combustion*, T. Lieuwen, Yang, V., Editor. To Appear.
16. Gouldin, F., Cheng, R.K. *International Workshop on Premixed Turbulent Flames*. [cited; Available from: http://eetd.lbl.gov/aet/combustion/workshop/workshop.html.
17. Videto, B.D., Santavicca, D. A., *A Turbulent Flow System for Studying Turbulent Combustion Processes.* Combustion Science and Technology, 1991. **76**(1-3): p. 159-164.
18. Bédat, B., Cheng, R. K., *Experimental Study of Premixed Flames in Intense Isotropic Turbulence.* Combustion and Flame, 1995. **100**(3): p. 485-494.
19. Kortschik, C., T. Plessing, and N. Peters, *Laser Optical Investigation of Turbulent Transport of Temperature Ahead of the Preheat Zone in a Premixed Flame.* Combustion and Flame, 2004. **136**(1-2): p. 43-50.
20. Mayo Jr, W.T. *A Discussion of Limitations and Extentions of Power Spectrum Estimation with Burst-Counter LDV Systems*. in *International Workshop on Laser Velocimetry*. 1974. West Lafayette, Indiana, Purdue University.
21. Tummers, M.J., Passchier, D. M., *Spectral Estimation Using a Variable Window and the Slotting Technique*

with Local Normalization. Measurement Science and Technology, 1996. **7**: p. 1541-1546.

22. Dasch, C., *One-Dimensional Tomography- A Comparison of Abel, Onion-Peeling, and Filtered Backprojection Methods.* Applied Optics, 1992. **31**(8): p. 1146–1152.

23. Smallwood, G.J., Gülder, Ö L., Snelling, D. R., Deschamps, B. M., Gökalp, I., *Characterization of Flame Front Surfaces in Turbulent Premixed Methane/Air Combustion.* Combustion and Flame, 1995. **101**(4): p. 461-470.

24. Davis, S.G., Joshi, A. V., Wang, H., Egolfopoulos, F., *An Optimized Kinetic Model of H2/CO Combustion.* Proceedings of the Combustion Institute, 2005. **30**(1): p. 1283-1292.

25. Bradley, D., *How Fast Can We Burn?* Symposium (International) on Combustion, 1992. **24**(1): p. 247-262.

26. Anand, M.S., Pope, S. B., *Calculations of Premixed Turbulent Flames by PDF Methods.* Combustion and Flame, 1987. **67**(2): p. 127-142.

27. Schelkin, K.I., *On Combustion in Turbulent Flow.* Zh. Tekh. Fiz, 1943. **13**: p. 520-530.

28. Yakhot, V., *Propagation Velocity of Premixed Turbulent Flames.* Combustion Science and Technology, 1988. **60**(1): p. 191-214.

29. Kobayashi, H., *Experimental Study of High-Pressure Turbulent Premixed Flames.* Experimental Thermal and Fluid Science, 2002. **26**(2-4): p. 375-387.

30. Kido, H., Nakahara, M., Hashimoto, J., Barat, D., *Turbulent Burning Velocities of Two-Component Fuel Mixtures of Methane, Propane and Hydrogen.* JSME International Journal Series B, 2002. **45**(2): p. 355-362.

31. Nakahara, M., Kido, H., *A Study of the Premixed Turbulent Combustion Mechanism Taking the Preferential Diffusion Effect into Consideration* Memoirs of the Faculty of Engineering, Kyushu University, 1998. **58**(2): p. 55-82.